



**HAL**  
open science

## Coupled spin cross-over and ferroelasticity: revisiting the prototype $[\text{Fe}(\text{ptz})(6)](\text{BF}_4)(2)$ material

Eric Collet, Giovanni Azzolina, Jelena Jeftić, Marie-Hélène Lemée-Cailleau

### ► To cite this version:

Eric Collet, Giovanni Azzolina, Jelena Jeftić, Marie-Hélène Lemée-Cailleau. Coupled spin cross-over and ferroelasticity: revisiting the prototype  $[\text{Fe}(\text{ptz})(6)](\text{BF}_4)(2)$  material. *Advances in Physics: X*, 2023, 8 (1), pp.2161936. 10.1080/23746149.2022.2161936 . hal-03969207

**HAL Id: hal-03969207**

**<https://hal.science/hal-03969207>**

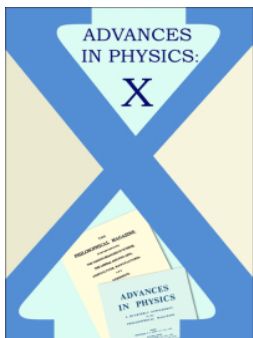
Submitted on 30 May 2023

**HAL** is a multi-disciplinary open access archive for the deposit and dissemination of scientific research documents, whether they are published or not. The documents may come from teaching and research institutions in France or abroad, or from public or private research centers.

L'archive ouverte pluridisciplinaire **HAL**, est destinée au dépôt et à la diffusion de documents scientifiques de niveau recherche, publiés ou non, émanant des établissements d'enseignement et de recherche français ou étrangers, des laboratoires publics ou privés.



Distributed under a Creative Commons Attribution 4.0 International License



## Coupled spin cross-over and ferroelasticity: revisiting the prototype $[\text{Fe}(\text{ptz})_6](\text{BF}_4)_2$ material

Eric Collet, Giovanni Azzolina, Jelena Jeftić & Marie-Hélène Lemée-Cailleau

To cite this article: Eric Collet, Giovanni Azzolina, Jelena Jeftić & Marie-Hélène Lemée-Cailleau (2023) Coupled spin cross-over and ferroelasticity: revisiting the prototype  $[\text{Fe}(\text{ptz})_6](\text{BF}_4)_2$  material, *Advances in Physics: X*, 8:1, 2161936, DOI: [10.1080/23746149.2022.2161936](https://doi.org/10.1080/23746149.2022.2161936)

To link to this article: <https://doi.org/10.1080/23746149.2022.2161936>



© 2023 The Author(s). Published by Informa UK Limited, trading as Taylor & Francis Group.



Published online: 01 Jan 2023.



Submit your article to this journal [↗](#)



Article views: 684



View related articles [↗](#)







View Crossmark data [↗](#)

REVIEW

 OPEN ACCESS



## Coupled spin cross-over and ferroelasticity: revisiting the prototype $[\text{Fe}(\text{ptz})_6](\text{BF}_4)_2$ material

Eric Collet <sup>a,b</sup>, Giovanni Azzolina <sup>a</sup>, Jelena Jeftić <sup>c</sup> and Marie-Hélène Lemée-Cailleau <sup>d</sup>

<sup>a</sup>Univ Rennes, CNRS, IPR (Institut de Physique de Rennes), Rennes, France; <sup>b</sup>Department of Chemistry, DYNACOM IRL2015 University of Tokyo- CNRS - UR1, Tokyo, Japan; <sup>c</sup>Univ Rennes, CNRS, ENSCR, ISCR (Institut des Sciences Chimiques de Rennes), Rennes, France; <sup>d</sup>Institut Laue-Langevin, France

### ABSTRACT

Spin-crossover (SCO) materials exhibit thermal conversion from low to high-spin states. We review different models developed to describe this entropy-driven process and the occurrence of cooperative conversions resulting from elastic interactions. There is a growing number of SCO materials exhibiting unusual thermal conversions when symmetry breaking occurs. To illustrate the importance of considering both phenomena, we review studies of the prototype  $[\text{Fe}(\text{ptz})_6](\text{BF}_4)_2$  system, exhibiting at atmospheric pressure a single step thermal transition with hysteresis, where a ferroelastic distortion occurs from the high-spin high-symmetry (HShs) phase, towards the low-spin low-symmetry (LSls) phase. Under pressure, sequential conversions occur on cooling from the HShs phase towards a high-spin low-symmetry (HSls) phase, followed by a spin crossover towards the LSls phase. In addition, a metastable low-spin high-symmetry (LSHs) state forms upon fast cooling. We revisit this coupling and decoupling of spin crossover and ferroelastic phase transition through the Landau theory model adapted by Collet, which provides qualitative agreement with the experimental data, such as the phase diagram and the evolution of spin transition curves or lattice deformations under pressure. This Ferroelastic Instability coupled to Spin Crossover (FISCO) approach should be generalized to many materials undergoing coupled spin transition and symmetry breaking.

### ARTICLE HISTORY

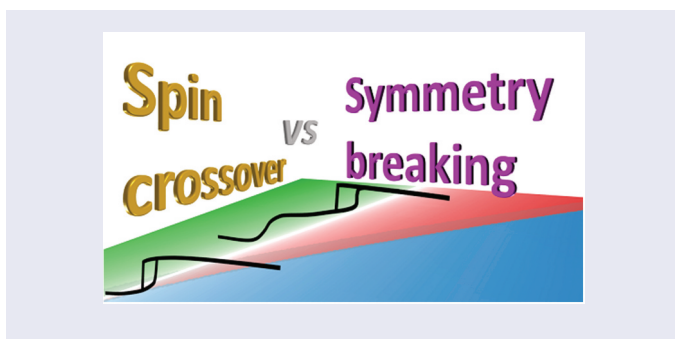
Received 14 October 2022  
Revised 13 November 2022  
Accepted 19 December 2022

### KEYWORDS

Spin-crossover; symmetry breaking; phase diagram; ferroelasticity; molecular magnetism

**CONTACT** Eric Collet  [eric.collet@univ-rennes1.fr](mailto:eric.collet@univ-rennes1.fr)  Univ Rennes, CNRS, IPR (Institut de Physique de Rennes), UMR 6251, Rennes F-35000, France

© 2023 The Author(s). Published by Informa UK Limited, trading as Taylor & Francis Group.  
This is an Open Access article distributed under the terms of the Creative Commons Attribution License (<http://creativecommons.org/licenses/by/4.0/>), which permits unrestricted use, distribution, and reproduction in any medium, provided the original work is properly cited.



## Introduction

Electronic multistability in molecular-based materials, such as spin-crossover (SCO) [1–4], or charge-transfer systems [5–8], is at the origin of the development of new functions and applications [9–11]. Since the different electronic states have different entropy and volume, phase transitions may occur at thermal equilibrium driven by temperature – pressure [12–21], or inclusion of guests [22,23]. External stimuli such as magnetic field, electric field or light [8,24–30], allow efficient control of molecular spin state down to ultrafast time-scale [31–36]. In crystals, the elastic coupling between volume-changing molecules can drive cooperative conversions at thermal equilibrium [25,37–41] or under light excitation [42–51]. For SCO, different models [25,40,52–56] used an Ising variable  $q_i$  to describe the high-spin (HS,  $q_i = 1$ ) or low-spin (LS,  $q_i = -1$ ) state of the  $i^{\text{th}}$  molecular site and monitor spin conversion curves through the average value of  $q$  or the HS fraction  $\gamma$ :

$$q = \frac{N_{HS} - N_{LS}}{N_{HS} + N_{LS}} \quad \text{or} \quad \gamma = \frac{N_{HS}}{N_{HS} + N_{LS}} \quad \text{with} \quad \gamma = \frac{q + 1}{2} \quad (1)$$

$N_{HS}$  and  $N_{LS}$  denote the number of sites in high-spin (HS) or low-spin (LS) states. A spin crossover is a gradual evolution of the HS fraction from  $\gamma = 0$  ( $q = -1$ ) to  $\gamma = 1$  ( $q = 1$ ), while a discontinuous evolution, eventually associated with a thermal hysteresis, corresponds to a spin transition [57,58].

The thermodynamical aspects of SCO have been largely described through various models, taking into account crystal field theory, entropy or elastic interactions to name a few [2,3,25,39,46,53,56,59–61]. The popular Slichter-Drickamer model is used to characterize the degree of cooperativity during spin conversions [56,62]. It describes the Gibbs energy  $G$  of the system as a weighted contribution of the HS ( $G_{HS}$ ) and LS ( $G_{LS}$ ) species, and it includes a mixing entropy ( $S_{mix}$ ) and intermolecular coupling through the parameter  $\Gamma$ :

$$G = \gamma G_{HS} + (1 - \gamma) G_{LS} - TS_{mix} + \Gamma \gamma (1 - \gamma) \quad (2)$$

Spiering highlighted the key role of elastic interaction in spin-crossover materials[63]. Weak  $\Gamma$  corresponds to continuous spin crossover, while large  $\Gamma$  corresponds to spin transition.

Recently, more complex elastic models were introduced for reproducing nucleation and propagation of HS and LS phases or cluster formation [40,52,64]. The elastic Ising-like Hamiltonian [60] includes, on the one hand, a thermodynamical part, with energy difference  $D$  and degeneracy ratio  $g$  between HS and LS states, and, on the other hand, an elastic potential, taking into account elastic interaction between constituting molecules and volume change associated with spin conversion:

$$H = \frac{1}{2} \sum_i (D - kT \ln g) q_i + \sum_{\langle i,j \rangle} V_{ij}^{inter} \quad (3)$$

As recently reviewed, such sophisticated description of the elastic potential account for lattice dynamics and finite size effects in molecular spin crossover systems and out-of-equilibrium dynamics[40]. Additional models including ferro- and anti-ferro-elastic couplings were used to describe stepwise conversion and the formation of spin-state concentration waves, where the HS fraction is spatially modulated [41,52,53,65–70].

An interesting case study is the prototype  $[\text{Fe}(\text{ptz})_6](\text{BF}_4)_2$  material, which was intensively investigated [71–78]. At atmospheric pressure, Gülich reported an unsymmetric spin transition thermal hysteresis[71], from the HS high-symmetry (HS)  $R\bar{3}$  phase, towards the LS low-symmetry (LS)  $P\bar{1}$  phase. Therefore  $[\text{Fe}(\text{ptz})_6](\text{BF}_4)_2$  is a ferroelastic material, as ferroelasticity is a phenomenon in which a symmetry-breaking phase transition occurs between different crystalline systems: rhombohedral  $R\bar{3}$  and triclinic  $P\bar{1}$  in the present case [79,80]. Under pressure, it was shown that the spin-state conversion decouples from the ferroelastic  $R\bar{3} \rightarrow P\bar{1}$  ferroelastic phase transition and the SCO and symmetry-breaking transition occur sequentially [14,81,82]. In order to address the basic problem of spin-state conversion coupled to symmetry-breaking and explain the different thermal transition curves on warming from the LS phase or cooling from the HS phase, Hauser proposed a new approach[83]. He included in the Slichter-Drickamer model an additional contribution to Gibbs free energies from the symmetry change in the LS phase, and different interaction terms  $\Gamma$  between HS and LS states. This allowed better matching with experimental data.

Complex spin conversion curves appear when SCO couples to symmetry breaking[84], which influences the hysteretic behavior in term of broadening and shape [78,85–97]. Indeed, when a ferroelastic phase transition occurs [79,80], the symmetry breaking couples to the strains and can

therefore affect spin conversion [98,99] or out-of-equilibrium HS  $\rightarrow$  LS relaxation [83,100]. In addition, coupled SCO and symmetry-breaking also allow for the emergence of functions, such as ferro- or ferri-magnetism, ferroelectricity or ferroelasticity [7,101–106], or additional control through magneto-electric [29,30]. However, these phenomena can't be explained by the above-mentioned models, not considering explicitly symmetry breaking.

In this paper, we revisit the coupling and decoupling of spin crossover and ferroelastic phase transition in the  $[\text{Fe}(\text{ptz})_6](\text{BF}_4)_2$  material with a new light on previously published experimental data [14,78,83]. We use the theoretical model proposed by Collet, based on the Landau theory, and accounting for both spin-crossover phenomena and considering the elastic coupling between SCO and symmetry breaking [84,89,99]. This Ferroelastic Instability coupled to Spin Crossover (FISCO) approach provides qualitative agreement with the experimental data, such as the phase diagram and the evolution of spin transition curves or lattice deformations under pressure.

## Materials and methods

We revisit the phase diagram of  $[\text{Fe}(\text{ptz})_6](\text{BF}_4)_2$  and review previous experimental data, showing that spin crossover and ferroelastic transition can occur simultaneously or sequentially. We show in Figure 1 spin transition curves obtained from single-crystal optical spectra absorption data, as published by Jeftić and Hauser[83]. We show in Figure 2 the strain tensor  $\varepsilon_{11}(T) = \frac{a_{LT}(T)}{a_{HT}(T)} - 1$  at 1 bar and 1000 bars, as introduced hereafter. As explained by Carpenter[79],  $a_{HT}(T)$  corresponds to the lattice parameters measured in the high-spin high-symmetry phase and extrapolated in the low-spin low-symmetry phase, which accounts for thermal expansion (or compressibility) of the high-spin high-symmetry phase. For the data at 1000 bars we used data from references 14, with a second order fit of  $a_{HT}(T)$  above 198 K, where the ferroelastic phase transition occurs on cooling from the HShs phase, to extrapolate  $a_{HT}(T)$  below 198 K and calculate  $\varepsilon_{11}(T)$  from the measured  $a_{LT}(T)$ . For the data at 1 bar we used data from references 78 and used 150 K as reference. We use the Landau theory of phase transition, adapted by Collet et al for spin-crossover phenomena [84,89,99], to rationalize how the elastic coupling between non-symmetry-breaking spin crossover and symmetry-breaking structural distortions affect spin conversion curves.

## Results

The  $[\text{Fe}(\text{ptz})_6](\text{BF}_4)_2$  iron(II) spin-crossover compound exhibits at atmospheric pressure a spin-transition hysteresis loop shown in Figure 1a, where

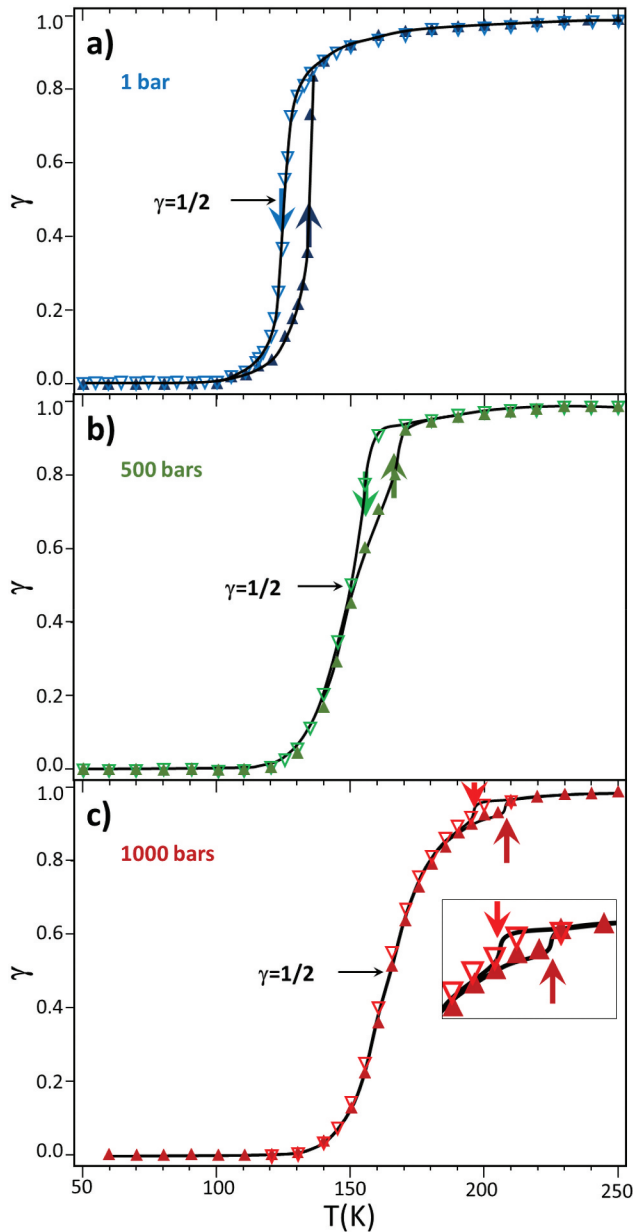


**Figure 1.** Spin state conversion curves of the high-spin fraction  $\gamma$  of the system  $[\text{Fe}(\text{ptz})_6](\text{BF}_4)_2$  at pressures of 1 bar (a), 500 bars (b), and 1000 bars (c) measured on warming ( $\blacktriangle$ ) and cooling ( $\blacktriangledown$ ) modes. The data are replotted from reference 81. The thermal hysteresis due to the ferroelastic phase transition from  $R\bar{3}$  at high temperature to  $P\bar{1}$  at low temperature is indicated by arrows.

the evolution of the fraction  $\gamma$  of HS molecules was monitored by optical spectroscopy[83]. This change of spin state is coupled with a ferroelastic phase transition from the high temperature HSs  $R\bar{3}$  space group to the low temperature LSs  $P\bar{1}$  space group [72,107,108]. The hysteresis loop is about

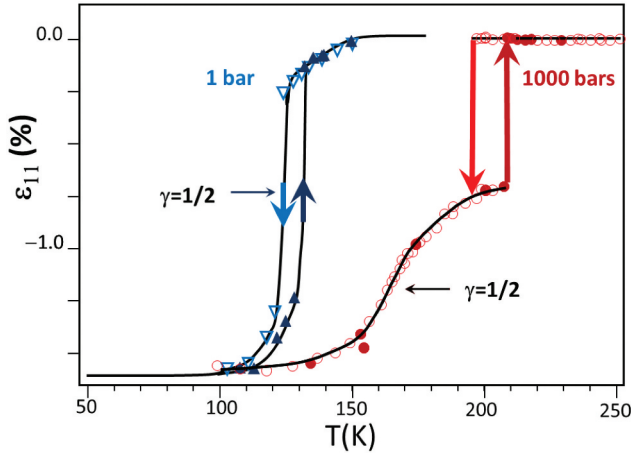


**Figure 2.** Thermal dependence of the volume strain component  $\varepsilon_{11}$  at 1 bar on warming ( $\blacktriangle$ ) and cooling ( $\blacktriangledown$ ) and 1000 bars on warming ( $\bullet$ ) and cooling ( $\circ$ ). Data are extrapolated from references 78 and 14. The points corresponding to  $\gamma = 1/2$  in Figure 1 are indicated by the arrows.

7 K wide at atmospheric pressure and unsymmetric, with a more discontinuous cooling branch around  $T_c^\downarrow = 128$  K and a more gradual warming branch around  $T_c^\uparrow = 135$  K [71–73,75–77]. The symmetry breaking of the crystalline lattice is responsible for the appearance of the ferroelastic domains, which induces cracks or defects [74]. Upon fast cooling, the ferroelastic phase transition is suppressed: the LS crystal remains in the  $R\bar{3}$  space group [109–111]. As reviewed by Carpenter [79], in addition to symmetry breaking, ferroelastic phase transitions are also characterized by the thermal dependence of the spontaneous volume strain  $v_s(T) = \frac{V_{LT}(T)}{V_{HT}(T)} - 1$ , where  $V_{LT}(T)$  is the volume of the low temperature phase and  $V_{HT}(T)$  the HT one, extrapolated at low temperature  $T$ . The volume strain  $v_s$  is also given by the components of the spontaneous strain tensor  $v_s = \varepsilon_{11} + \varepsilon_{22} + \varepsilon_{33}$ .

Wiehl *et al* used powder diffraction measurements to describe in detail the ferroelastic nature of the phase transition of  $[\text{Fe}(\text{ptz})_6](\text{BF}_4)_2$ , through the lattice deformations responsible for the non-symmetry breaking volume strain  $v_s$  and the symmetry-breaking strain tensor [108]. During the  $R\bar{3} \rightarrow P\bar{1}$  symmetry-breaking the  $\bar{3}$  axis is lost: the  $a$  and  $b$  crystalline axis differ and the  $\alpha$  and  $\beta$  angles deviate from  $90^\circ$  and  $\gamma$  from  $120^\circ$ . Because of the formation of ferroelastic domains in the LS phase, it is not easy to monitor all these deformations on single crystal. In Figure 2 we show the non-symmetry-breaking component of the strain tensor  $\varepsilon_{11} = \frac{a_{LT}(T)}{a_{HT}(T)} - 1$  calculated from the data published in a previous paper, as explained above [78]. At 1 bar, we can see pretransitional evolution of  $\varepsilon_{11}$  and therefore  $v_s$  on



approaching the phase transition, both on warming and on cooling. Wiehl also reported that the lattice parameter  $a$  expands on cooling from room temperature down to 150 K, where a weak lattice contraction starts, while on warming from low temperature there is no thermal expansion up to 100 K and a weak expansion on approaching the phase transition [108]. Both pretransitional evolution of the lattice are due to the partial spin conversion on approaching the phase transition, as monitored by optical spectroscopy (Figure 1a).

Since both spin crossover and ferroelastic distortion phenomena strongly couple to volume change, pressure studies play an important role for understanding their relative contributions. Single-crystal absorption spectra studies performed by Jeftić [83], revealed that the shapes of the thermal spin conversion strongly change with pressure. The transition curves at 500 bars (Figure 1b) exhibit two different regions. Below 150 K, which almost corresponds to the half conversion temperature ( $\gamma = \frac{1}{2}$ ), the warming and cooling curves superpose perfectly and the spin state conversion is of spin-crossover type. However, compared to 1 bar, the thermal hysteresis appears at higher temperatures, and is characterized by two substantially smaller jumps of  $\gamma$  than at  $T_c^\downarrow = 158$  K and  $T_c^\uparrow = 168$  K. The 1000 bars curve exhibit a spin-crossover up to 198 K, while even smaller jumps of  $\gamma$  occurs at  $T_c^\downarrow = 198$  K on cooling and  $T_c^\uparrow = 210$  K on warming. The half conversion is around 165 K, well below the thermal hysteresis due to the ferroelastic transition. These results show that pressure affects differently the ferroelastic phase transition and the spin crossover, which decouple under pressure.

A recent study by Chakraborty et al [112] allows comparing the relative contribution of the ferroelastic phase transition and SCO to the volume contraction. For the  $[\text{Fe}(\text{ptz})_6](\text{BF}_4)_2$  compound, their data reveal a volume strain  $\nu_s = -0.058(1)$  from HShs to LSls, normalized to the number of formula unit  $Z$  per unit cell, including therefore contributions from both SCO and ferroelastic distortion. The volume strain due to the SCO between the HShs phase and the LSls phase, thermally quenched at 84 K, is  $\nu_{SCO} = -0.028(1)$ . The volume strain due to the only ferroelastic distortion between LSls phase and the HShs phase is  $\nu_{SF} = -0.031(1)$ . For the pure  $[\text{Ru}(\text{ptz})_6](\text{BF}_4)_2$  compound, which does not exhibit SCO, there is a similar volume strain  $\nu_{SF} = -0.028(1)$ , only due to the  $R\bar{3} \leftrightarrow P\bar{1}$  ferroelastic distortion. This study confirms that the amplitude of the contribution to the volume strain  $\nu_s$  of  $\nu_{SF}$  and  $\nu_{SCO}$  are quite similar.

The neutron diffraction studies of  $[\text{Fe}(\text{ptz})_6](\text{BF}_4)_2$  provide additional evidences of the dissociation of ferroelastic transition from spin crossover [81]. Three phases are reported in a  $(P, T)$  phase diagram: the HShs phase ( $R\bar{3}$ ), the LSls ( $P\bar{1}$ ), and the intermediate high-spin low-symmetry  $P\bar{1}$  phase (HSlS). Above the triple point, like at 1000 bars, the sequence of phase transitions is characterized by the evolution of the lattice parameter

*a* exhibiting a discontinuous hysteretic behavior at 198 and 210 K and a gradual evolution around 165 K[14]. Figure 2 shows the component  $\varepsilon_{11}$  of the strain tensor calculated from these data, as explained in the materials and method section. The first-order ferroelastic transition HSs ( $R\bar{3}$ )  $\rightarrow$  HSls ( $P\bar{1}$ ) is characterized by discontinuous lattice contraction at  $T_c^\downarrow = 198$  K on cooling and expansion at  $T_c^\uparrow = 210$  K on warming. In addition, there is a distinct broad and continuous lattice contraction centered at 165 K, which accompanies the spin crossover between the HSls ( $P\bar{1}$ ) and the LSls ( $P\bar{1}$ ) phases. The thermal evolution of  $\varepsilon_{11}$  obtained from neutron diffraction experiments at 1000 bars exhibits characteristic temperatures of the hysteresis for the ferroelastic phase transition and of the spin crossover in perfect agreement with optical spectroscopy data (Figure 1c). The fact that  $\varepsilon_{11}$  exhibits almost no thermal contraction at 1000 bars on cooling from 300 K down to 198 K is also consistent with optical data showing that the systems remains almost fully HS in this temperature range, while the contractions due to the  $R\bar{3} \rightarrow P\bar{1}$  phase transition and HS  $\rightarrow$  LS crossover are clearly separated. Interestingly, both phenomena contribute on an equal footing to the volume strain, as the two contractions of  $\varepsilon_{11}$  accompanying the ferroelastic transition and the SCO have similar amplitudes. The spin-state conversion cooperativity is therefore strongly affected by the ferroelastic phase transition.

## Discussion

For rationalizing these observations, we use the Ferroelastic Instability coupled to Spin Crossover (FISCO) approach proposed by Collet [84,89,99], which allows understanding the thermal dependence and the coupling between the symmetry breaking order parameter  $\eta$  and the non-symmetry breaking change of the HS fraction  $\gamma$ . In the case of  $[\text{Fe}(\text{ptz})_6](\text{BF}_4)_2$ , the symmetry-breaking order parameter  $\eta$  driving the  $R\bar{3} \rightarrow P\bar{1}$  ferroelastic transition belongs to the bidimensional  $E_g$  representation of the  $\bar{3}$  point group, the basis of which is built with two distortion strains, [113–116] as it is also the case for cubic  $\rightarrow$  tetragonal ferroelastic transition of the RbMnFe system [89]. The simplest symmetry-adapted Landau potential for describing coupled symmetry-breaking and SCO for  $[\text{Fe}(\text{ptz})_6](\text{BF}_4)_2$  takes the following form

$$G(q, \eta) = \frac{1}{2}a\eta^2 + \frac{1}{3}b\eta^3 + \frac{1}{4}c\eta^4 + Aq + \frac{1}{2}Bq^2 + \frac{1}{4}Cq^4 + \frac{1}{2}C_s^0 v_s^2 + \lambda_\eta v_s \eta^2 + \lambda_q v_s \left( \frac{1-q}{2} \right) \quad (4)$$

For limiting the number of parameters, we will consider hereafter  $b$ ,  $c$ ,  $B$  and  $C$  constant. The  $\eta^2, \eta^3, \eta^4$  terms describe the symmetry breaking potential, with  $a = a_0(T - T_{SB})$ .  $c > 0$  for stability [80]. The coefficient  $a$  changes sign with temperature  $T$  at  $T_{SB}$ , which stabilizes  $\eta = 0$  above  $T_{SB}$  and  $\eta \neq 0$  below, while the symmetry-allowed  $\eta^3$  term limits the  $R\bar{3} \rightarrow P\bar{1}$  ferroelastic transition to first-order only. The  $q, q^2, q^4$ , terms describe the spin conversion potential with  $A = A_0(T_{SC} - T)$  and  $C > 0$  for stability [117]. Here we use  $B > 0$ , which corresponds to a spin-crossover, with a gradual change from HS ( $q > 0$ ) above  $T_{SC}$  to LS ( $q < 0$ ) below [84]. A key point of this model is that it includes the elastic energy  $\frac{1}{2} C_s^0 v_s^2$  related to elastic constant  $C_s^0$  and the total volume strain  $v_s$ , but also the elastic coupling to  $v_s$  of the ferroelastic distortion ( $\lambda v_s \eta^2$  is zero in high-symmetry phase) and of the spin state conversion ( $\lambda_q v_s (\frac{1-q}{2})$  is 0 taken as reference in the HS state where  $q = 1$ ). All these terms contribute to the equilibrium volume strain [89]:

$$v_s = - \frac{[\lambda_q (\frac{1-q}{2}) + \lambda_\eta \eta^2]}{C_s^0} \quad (5)$$

Substituting  $v_s$  in equation (2) results in a renormalization of some coefficients:

$$G(q, \eta) = \frac{1}{2} a_0 (T - T_{SB}) \eta^2 + \frac{1}{3} b \eta^3 + \frac{1}{4} c \eta^4 + A_0 (T_{SC} - T) q + \frac{1}{2} B q^2 + \frac{1}{4} C q^4 + D q \eta^2 \quad (6)$$

Here we use  $D > 0$  for stabilizing the LSls phase ( $q < 0$  and  $\eta \neq 0$ ).

Regarding the  $(P, T)$  phase diagram, we may consider that in addition to temperature, the coefficients  $a$  and  $A$  can also linearly depend on pressure:  $a = a_0(T - T_{SB}) + a_1(P - P_{SB})$  and  $A = A_0(T_{SC} - T) + A_1(P_{SC} - P)$ . It is also important to notice that the difference in the symmetry-breaking and spin-crossover temperature instabilities changes linearly with pressure:

$$T_{SB} - T_{SC} = - \frac{A + a}{a_0} + \frac{A_1}{a_0} P_{SC} - \frac{a_1}{a_0} P_{SB} + \frac{a_1 - A_1}{a_0} P \quad (7)$$

To avoid over-parametrization and -representation in a more complex space of parameters, we do not consider the pressure dependence of  $a$  and  $A$ . In this simplest approximation,  $(T_{SB} - T_{SC})$  is therefore analogous to a pressure. The phase diagram shown in the  $(T_{SB} - T_{SC}, T - T_{SC})$  space is therefore analogous to  $(P, T)$ . In this way, we explore the different phases which may exist, characterized by their spin state (HS for  $q > 0$  or LS for  $q < 0$ ) and symmetry (hs for  $\eta = 0$  or ls for  $\eta \neq 0$ ). The equilibrium values of the order parameters characterize the stability region of the different phases and are numerically found by minimizing  $G(q, \eta)$  [84].

The ‘pressure-like’ axis ( $T_{SB}-T_{SC}$ ) and temperature axis ( $T-T_{SC}$ ), in [Figure 3](#) are scaled to fit the experimental phase diagram [81]. Around 1 bar the spin conversion and the symmetry breaking occur simultaneously, with a thermal hysteresis between the HShs and LSlS phases (grey shaded area between hs and ls phases). The phase diagram exhibits a triple point around (200 bars, 140 K), where the HShs, HSlS and LSlS phases coexist. Above the triple point, a ferroelastic phase transition from HShs to HSlS phases occurs around  $T_{SB}$ , followed at lower temperature by a spin crossover (dashed line) from the HSlS to the LSlS phase.

The hysteretic domain of bistability, shown by the grey area in between continuous lines in the phase diagram, is due to the  $(R\bar{3}) \rightarrow (P\bar{1})$  ferroelastic transition, as the bidimensional nature of the symmetry-breaking order parameter, restricts symmetry breaking to first-order transition [80,84,99].

[Figures 4a and 4b](#) show the temperature dependence of the order parameters  $\gamma(T)$  and  $\eta^2(T)$  in the calculated phase diagram for 1 bar, 500 bars and 1000 bars. The discontinuous change of  $\eta^2(T)$  characterizes the discontinuous ferroelastic transition and measures the deviation of the system from high symmetry. Below the triple point (1 bar),  $\gamma(T)$  and  $\eta^2(T)$  both change discontinuously and simultaneously whether heating or cooling and the spin transition curve mimics the unsymmetric hysteresis shown in

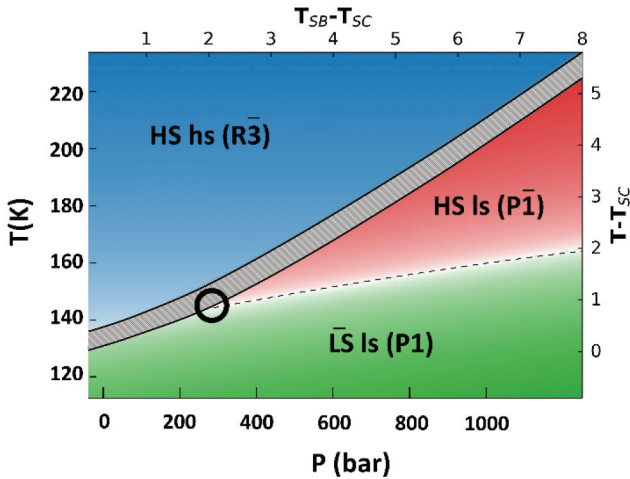


**Figure 3.** Calculated phase diagram of  $\text{Fe}(\text{ptz})_6(\text{BF}_4)_2$ , with scaled pressure-like ( $T_{SB}-T_{SC}$ ) and temperature ( $T-T_{SC}$ ) axes fitting experimental data from in ref 79. Below  $\approx 250$  bars, spin conversion and symmetry breaking occur simultaneously with a thermal hysteresis shown by the grey shaded area between the HShs ( $R\bar{3}$ ) and LSlS ( $P\bar{1}$ ) phases. At the triple point shown by the circle, located around (250 bars, 140 K), the HShs, LSlS and HSlS ( $P\bar{1}$ ) phases coexist. Above the triple point, a ferroelastic HShs ( $R\bar{3}$ )  $\rightarrow$  HSlS ( $P\bar{1}$ ) phase transition occurs at high temperature with a thermal hysteresis. At lower temperature, the spin crossover centered on the dashed line occurs from the HSlS ( $P\bar{1}$ ) and LSlS ( $P\bar{1}$ ) HSlS phases. The phase diagram was calculated for the potential (4) with  $b = -6$ ,  $c = 12$ ,  $B = 2$ ,  $C = 12$ ,  $D = 2$ .

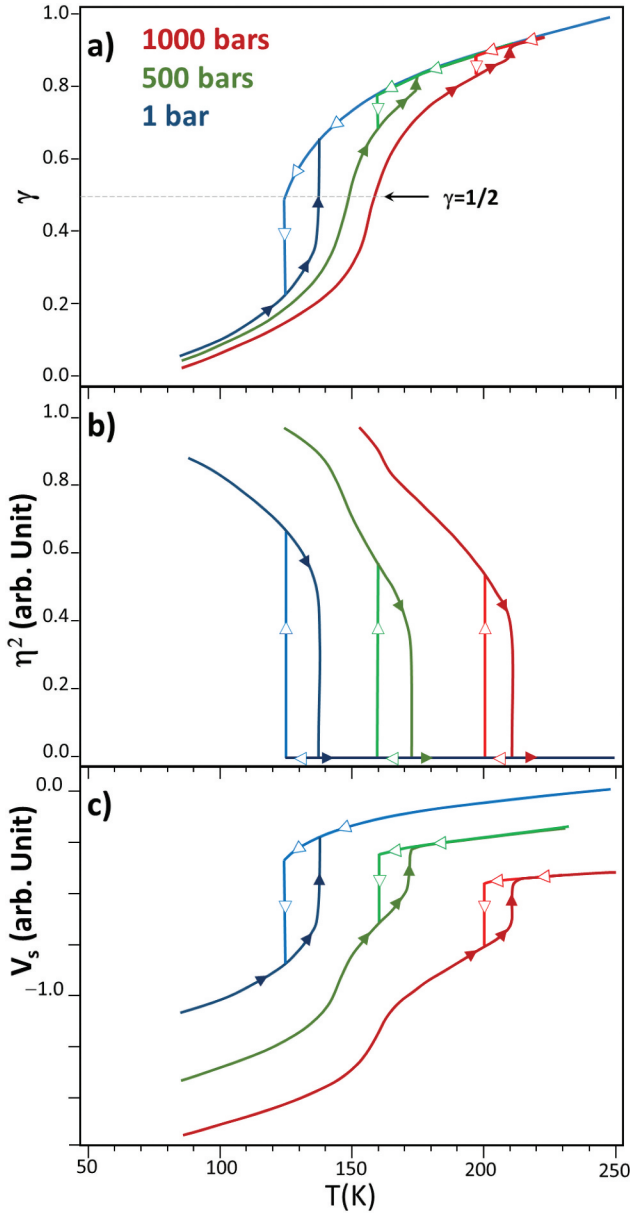


**Figure 4.** Thermal dependence of the spin transition curves  $\gamma(T)$  (a), the symmetry breaking curves  $\eta^2(T)$  (b), and the volume strain  $v_s$  (c) calculated for different ‘pressures’ ( $T_{SB}-T_{SC}$ ) corresponding to 1, 500 and 1000 bars. Volume strains are vertically shifted for clarity.

**Figure 1a.** This unsymmetric hysteresis loop, characteristic of different cooperativities in the HShs and LSLs phases, is due to the  $Dq\eta^2$  coupling. Indeed, in the HShs phase where  $\eta = 0$ , the potential reaches

$$G(q, 0) = A_0(T_{SC} - T)q + \frac{1}{2}Bq^2 + \frac{1}{4}Cq^4 \quad (8)$$

It differs therefore from potential in the LSIs phase, where  $\eta \neq 0$  (Eq 6), which includes the additional contribution to the Gibbs energy from the symmetry change. These results justify a posteriori Hauser's approach considering different Gibbs free energies and interaction terms in the HS and LS phases of the complex [82,83]. In addition, the coefficient  $A = a_0(T_{SC}-T)$  changing sign at the SCO temperature  $T_{SC}$  in the HShs phase is renormalized in the LSIs phase to  $(A + D\eta^2) = a_0(T_{SC}^L - T)$ . The SCO temperature  $T_{SC}$  on cooling from the HShs phase is different from the one on warming from the LSIs phase  $T_{SC}^L = T_{SC} + D\eta^2$ , and the symmetry breaking stabilizes the LS state towards higher temperature. On cooling from the HShs phase, the symmetry breaking ( $\eta \neq 0$ ) and spin transition occur simultaneously, while on warming from the LSIs phase ( $q < 0$ ), the coupling stabilizes the LSIs phase towards higher temperature and a gradual spin-state conversion starts, followed by the simultaneous and discontinuous changes of symmetry and spin state.

Above the triple point (500 and 1000 bars, Figure 4) there is a gradual evolution of  $\gamma(T)$  on warming, followed by a discontinuous change around  $T_{SB}$  where the symmetry change occurs, due to the coupling.  $\eta^2(T)$  changes discontinuously around  $T_{SB}$  and exhibits a continuous evolution around  $T_{SC}$ . The apparent stepwise spin conversion curves  $\gamma(T)$  results from a spin crossover around  $\gamma = 1/2$  and a discontinuous change at higher temperature due to the ferroelastic transition. Figure 4c shows the thermal dependence of the volume strain  $v_s$  calculated with equation (5) through the thermal dependence of  $\gamma$  and  $\eta^2$ , with equal amplitudes. At 1 bar the evolution of  $v_s$  on cooling just above the ferroelastic phase transition is due to the partial spin conversion, measured in Figure 1a.

At the phase transition, the discontinuous evolutions of  $\gamma$  and  $\eta^2$  results in a single global and discontinuous contraction. Below the phase transition, the lattice contraction is mainly due to the spin conversion, as the components of the symmetry-breaking strain tensor exhibit weak temperature dependence [108]. The behavior of the calculated  $v_s$  is in good agreement with the thermal dependence of  $\epsilon_{11}$  at 1 bar (Figure 2). Our model also mimics the stepwise lattice contraction measured by neutron diffraction above the triple point at 1000 bars, with a discontinuous and hysteretic change of  $v_s$  at the ferroelastic phase transition, and a gradual change without hysteresis around the spin crossover (Figure 2 vs 4c). At high pressure, when  $T_{SB}$  strongly differs from  $T_{SC}$ , the contributions of the non-symmetry-breaking and symmetry-breaking order parameters to the total volume strain are clearly separated, in agreement with experimental data.

## Conclusion

The FISCO approach (Ferroelastic Instability coupled to Spin Crossover) is a relevant method for understanding spin conversion curves in materials for

which spin-state conversion couples to ferroelastic lattice distortion. This model allows for describing and modeling the interplay between symmetry-breaking phase transitions and SCO and provides the necessary formalism for disentangling spin transition and symmetry breaking, as well as the associated volume strain. It is necessary to consider the coupling between two order parameters: the non-symmetry-breaking evolution of the HS fraction  $\gamma$ , also probed through the evolution of the deviation from half conversion  $q$ , and the symmetry breaking ferroelastic distortion  $\eta$ . The elastic coupling of each parameter to the volume strain results in a  $Dq\eta^2$  coupling, which can drive spin state switching and symmetry change simultaneously, or sequentially. This model, which successfully reproduces experimental phase diagrams and various features reported in several SCO materials [89,97,99], will be of interest for a growing number of systems found to exhibit coupled electronic instability and symmetry breaking. We have to underline that only equilibrium stationary states are considered in the framework of the Landau theory. Therefore, kinetic effects related to cooling or warming rate or to the metastable LShs state, reached on flash cooling, cannot be grasped with this model, which is not considering fluctuations around equilibrium or quasi-equilibrium state. Including symmetry-breaking aspects to kinetic spin-state switching models is therefore a promising route for future.

## Acknowledgments

E.C. acknowledge Agence Nationale de la Recherche for financial support undergrant, ANR-19-CE30-0004 ELECTROPHONE and the Fondation Rennes1 for funding. The authors thank the Association Française de Magnétisme Moléculaire. The authors would like to thank Andreas Hauser for fruitful discussions.

## Disclosure statement


No potential conflict of interest was reported by the author(s).

## Funding

This work was supported by the Agence Nationale de la Recherche [ANR-19-CE30-0004 ELECTROPHONE]; Fondation Rennes 1 [Semestre innovation].

## ORCID

Eric Collet  <http://orcid.org/0000-0003-0810-7411>

Giovanni Azzolina  <http://orcid.org/0000-0002-6318-9360>

Jelena Jeftić  <http://orcid.org/0000-0002-1221-7253>

Marie-Hélène Lemée-Cailleau  <http://orcid.org/0000-0001-8212-5226>

## References

- [1] Halcrow MA. Spin-crossover materials: properties and applications. Chichester: John Wiley & Sons, Ltd; 2013. p. 546.
- [2] Gutlich P, Hauser A, Spiering H. Thermal and optical switching of iron(II) complexes. *Angew Chem Int Edition Engl.* 1994; 33:2024–2054.
- [3] Bousseksou A, Molnar G, Salmon L, et al. Molecular spin crossover phenomenon: recent achievements and prospects. *Chem Soc Rev.* 2011;40:3313–3335.
- [4] Molnár G, Mikolasek M, Ridier K, et al. Molecular spin crossover materials: review of the lattice dynamical properties. *Ann Phys Berlin.* 2019;531:1900076.
- [5] Tokoro H, Ohkoshi S. Multifunctional material: bistable metal–cyanide polymer of rubidium manganese hexacyanoferrate. *Bull Chem Soc Jpn.* 2015;88:227–239.
- [6] Meng YS, Sato O, Liu T. Manipulating metal-to-metal charge transfer for materials with switchable functionality. *Angew Chem Int Ed Engl.* 2018;57:12216–12226.
- [7] Pardo E, Train C, Liu H, et al. Multiferroics by rational design: implementing ferroelectricity in molecule-based magnets. *Angew Chem.* 2012;124:8481–8485.
- [8] Aguila D, Prado Y, Koumoussi ES, et al. Switchable Fe/Co prussian blue networks and molecular analogues. *Chem Soc Rev.* 2016;45:203–224.
- [9] Bellec A, Lagoute J, Repain V. Molecular electronics: scanning tunneling microscopy and single-molecule devices. *Cr Chim.* 2018;21:1287–1299.
- [10] Molnár G, Rat S, Salmon L, et al. Spin crossover nanomaterials: from fundamental concepts to devices. *Adv Mater.* 2018;30:1703862.
- [11] Manrique-Juárez MD, Mathieu F, Laborde A, et al. Micromachining-compatible, facile fabrication of polymer nanocomposite spin crossover actuators. *Adv Funct Mater.* 2018;28:1801970.
- [12] Vallone SP, Tantillo AN, Dos Santos AM, et al. Giant barocaloric effect at the spin crossover transition of a molecular crystal. *Adv Mater.* 2019;31:1807334.
- [13] Gaspar AB, Molnár G, Rotaru A, et al. Pressure effect investigations on spin-crossover coordination compounds. *Cr Chim.* 2018;21:1095–1120.
- [14] Lemée-Cailleau MH, Ecolivet C, Ouladdiaf B, et al. Intermediate ferroelastic phase of the photo-sensible spin-crossover system  $[\text{Fe}(\text{ptz})_6](\text{BF}_4)_2$ . *J Magn Magn Mater.* 2007;310:1792–1793.
- [15] Cafun JD, Lejeune J, Baudelet F, et al. Room-temperature photoinduced electron transfer in a Prussian blue analogue under hydrostatic pressure. *Angew Chem Int Ed Engl.* 2012;51:9146–9148.
- [16] Tailleux E, Marchivie M, Itie JP, et al. Pressure-induced spin-crossover features at variable temperature revealed by in situ synchrotron powder x-ray diffraction. *Chemistry.* 2018;24:14495–14499.
- [17] Paradis N, Le Gac F, Guionneau P, et al. Effects of internal and external pressure on the  $[\text{Fe}(\text{PM-PEA})_2(\text{NCS})_2]$  spin-crossover compound (with PM-PEA = N-(2'-pyridylmethylene)-4-(phenylethynyl)aniline). *Magnetochemistry.* 2016;2:15.
- [18] Miller RG, Narayanaswamy S, Clark SM, et al. Pressure induced separation of phase-transition-triggered-abrupt vs. gradual components of spin crossover. *Dalton Trans.* 2015;44:20843–20849.
- [19] Guionneau P. Crystallography and spin-crossover. A view of breathing materials. *Dalton Trans.* 2014;43:382–393.
- [20] Tissot A, Shepherd HJ, Toupet L, et al. Temperature- and pressure-induced switching of the molecular spin state of an orthorhombic iron(III) spin-crossover salt. *Eur J Inorg Chem.* 2013;2:1001–1008.



- [21] Li R, Levchenko G, Valverde-Muñoz FJ, et al. Pressure tunable electronic bistability in Fe(II) Hofmann-like two-dimensional coordination polymer [Fe(Fpz)<sub>2</sub>Pt(CN)<sub>4</sub>]: a comprehensive experimental and theoretical study. *Inorg Chem.* **2021**;60:16016–16028.
- [22] Piñeiro-López L, Valverde-Muñoz F-J, Trzop E, et al. Guest induced reversible on–off switching of elastic frustration in a 3D spin crossover coordination polymer with room temperature hysteretic behaviour. *Chem Sci.* **2021**;12:1317–1326.
- [23] Zenere KA, Duyker SG, Trzop E, et al. Increasing spin crossover cooperativity in 2D Hofmann-type materials with guest molecule removal. *Chem Sci.* **2018**;9:5623–5629.
- [24] Sato O. Dynamic molecular crystals with switchable physical properties. *Nat Chem.* **2016**;8:644–656.
- [25] Spiering H, Boukheddaden K, Linares J, et al. Total free energy of a spin-crossover molecular system. *Phys Rev B.* **2004**;70:184106.
- [26] Ozaki N, Tokoro H, Hamada Y, et al. Photoinduced magnetization with a high curie temperature and a large coercive field in a Co-W bimetallic assembly. *Adv Funct Mater.* **2012**;22:2089–2093.
- [27] Decurtins S, Gütllich P, Köhler CP, et al. Light-induced excited spin state trapping in a transition-metal complex: the hexa-1-propyltetrazole-iron (II) tetrafluoroborate spin-crossover system. *Chem Phys Lett.* **1984**;105:1–4.
- [28] Hauser A, Adler P, Deisenroth S, et al., Intersystem crossing in Fe(II) coordination-compounds. *Hyperfine Interact.* **1994**. 90:77–87.
- [29] Jakobsen VB, Trzop E, Dobbelaar E, et al. Domain wall dynamics in a ferroelastic spin crossover complex with giant magnetoelectric coupling. *J Am Chem Soc.* **2022**;144:195–211.
- [30] Dobbelaar E, Jakobsen VB, Trzop E, et al. Thermal and magnetic field switching in a two-step hysteretic MnIII spin crossover compound coupled to symmetry breakings. *Angew Chem.* **2022**;61:e202114021.
- [31] Cammarata M, Zerdane S, Balducci L, et al. Charge transfer driven by ultrafast spin transition in a CoFe Prussian blue analogue. *Nat Chem.* **2021**;13:10–14.
- [32] Azzolina G, Tokoro H, Imoto K, et al. Exploring ultrafast photoswitching pathways in RbMnFe prussian blue analogue. *Angew Chem.* **2021**;60:23267–23273.
- [33] Cammarata M, Bertoni R, Lorenc M, et al. Sequential activation of molecular breathing and bending during spin-crossover photoswitching revealed by femtosecond optical and X-Ray absorption spectroscopy. *Phys Rev Lett.* **2014**;113:227402.
- [34] Zerdane S, Wilbraham L, Cammarata M, et al. Comparison of structural dynamics and coherence of d-d and MLCT light-induced spin state trapping. *Chem Sci.* **2017**;8:4978–4986.
- [35] Barlow K, Johansson JO. Ultrafast photoinduced dynamics in prussian blue analogues. *Phys Chem Chem Phys.* **2021**;23:8118–8131.
- [36] Johansson JO, Kim JW, Allwright E, et al. Directly probing spin dynamics in a molecular magnet with femtosecond time-resolution. *Chem Sci.* **2016**;7:7061–7067.
- [37] Ksenofontov V, Spiering H, Schreiner A, et al. The influence of hydrostatic pressure on hysteresis phase transition in spin crossover compounds. *J Phys Chem Solids.* **1999**;60:393–399.
- [38] Hauser A, Jęfici J, Romstedt H, et al. Cooperative phenomena and light-induced bistability in iron(II) spin-crossover compounds. *Coord Chem Rev.* **1999**;192:471–491.
- [39] Spiering H, Willenbacher N. Elastic interaction of high-spin and low-spin complex molecules in spin-crossover compounds. II. *J Phys.* **1989**;1:10089.

- [40] Enachescu C, Nicolazzi W. Elastic models, lattice dynamics and finite size effects in molecular spin crossover systems. *Cr Chim.* **2018**;21:1179–1195.
- [41] Boukheddaden K, Miyashita S, Nishino M. Elastic interaction among transition metals in one-dimensional spin-crossover solids. *Phys Rev B.* **2007**;75. [10.1103/PhysRevB.75.094112](#)
- [42] Volte A, Mariette C, Bertoni R, et al., Dynamical limits for the molecular switching in a photoexcited material revealed by X-ray diffraction. *Commun Phys.* **2022**. 5:168.
- [43] Azzolina G, Bertoni R, Mariette C, et al. Out-of-equilibrium lattice response to photo-induced charge-transfer in a MnFe Prussian blue analogue. *J Mater Chem C.* **2021**;9:6773–6780.
- [44] Bertoni R, Collet E, Cailleau H, et al. Temperature dependence of the cooperative out-of-equilibrium elastic switching in a spin-crossover material. *Phys Chem Chem Phys.* **2019**;21:6606–6612.
- [45] Ridier K, Bas A-C, Shalabaeva V, et al. Finite size effects on the switching dynamics of spin-crossover thin films photoexcited by a femtosecond laser pulse. *Adv Mater.* **2019**;31:1901361.
- [46] Enachescu C, Stoleriu L, Nishino M, et al. Theoretical approach for elastically driven cooperative switching of spin-crossover compounds impacted by an ultrashort laser pulse. *Phys Rev B.* **2017**;95:224107.
- [47] Bertoni R, Lorenc M, Cailleau H, et al. Elastically driven cooperative response of a molecular material impacted by a laser pulse. *Nat Mater.* **2016**;15:606–610.
- [48] Bertoni R, Lorenc M, Graber T, et al. Cooperative elastic switching vs. laser heating in [Fe(phen)2(NCS)2] spin-crossover crystals excited by a laser pulse. *Crystengcomm.* **2016**;18:7269–7275.
- [49] Koshihara S, Ishikawa T, Okimoto Y, et al. Challenges for developing photo-induced phase transition (PIPT) systems: from classical (incoherent) to quantum (coherent) control of PIPT dynamics. *Phys Rep.* **2022**;942:1–61.
- [50] Jiang Y, Liu LC, Müller-Werkmeister HM, et al. Structural dynamics upon photo-excitation in a spin crossover crystal probed with femtosecond electron diffraction. *Angew Chem.* **2017**;56:7130–7134.
- [51] Field R, Liu LC, Gawelda W, et al. Spectral signatures of ultrafast spin crossover in single crystal [FeII(bpy)3](PF6)2. *Chem Eur J.* **2016**;22:5118–5122.
- [52] Watanabe H, Tanaka K, Bréfuel N, et al. Ordering phenomena of high-spin/low-spin states in stepwise spin-crossover materials described by the ANNNI model. *Phys Rev B.* **2016**;93:014419.
- [53] Paez-Espejo M, Sy M, Boukheddaden K. Elastic frustration causing two-step and multistep transitions in spin-crossover solids: emergence of complex antiferroelastic structures. *J Am Chem Soc.* **2016**;138:3202–3210.
- [54] Enachescu C, Nishino M, Miyashita S, et al. Shape effects on the cluster spreading process of spin-crossover compounds analyzed within an elastic model with Eden and Kawasaki dynamics. *Phys Rev B.* **2015**;91:104102.
- [55] Boukheddaden K, Shteto I, Hôo B, et al. Dynamical model for spin-crossover solids. II. Static and dynamic effects of light in the mean-field approach. *Phys Rev B.* **2000**;62:14806–14817.
- [56] Nicolazzi W, Bousseksou A. Thermodynamical aspects of the spin crossover phenomenon. *Cr Chim.* **2018**;21:1060–1074.
- [57] Buron-Le Cointe M, Hébert J, Baldé C, et al. Intermolecular control of thermoswitching and photoswitching phenomena in two spin-crossover polymorphs. *Phys Rev B.* **2012**;85:064114.

- [58] Gütlich P, Garcia Y, Spiering H. Spin transition phenomena. *Magn Mol Mater* IV. 2001; 271–344
- [59] Bousseksou A, McGarvey JJ, Varret F, et al. Raman spectroscopy of the high- and low-spin states of the spin crossover complex  $\text{Fe}(\text{phen})_2(\text{NCS})_2$ : an initial approach to estimation of vibrational contributions to the associated entropy change. *Chem Phys Lett*. 2000;318:409–416.
- [60] Pavlik J, Linares J. Microscopic models of spin crossover. *Cr Chim*. 2018;21:1170–1178.
- [61] Stoleriu L, Chakraborty P, Hauser A, et al. Thermal hysteresis in spin-crossover compounds studied within the mechanoelastic model and its potential application to nanoparticles. *Phys Rev B*. 2011;84:134102.
- [62] Slichter CP, Drickamer HG. Pressure-induced electronic changes in compounds of iron. *J Chem Phys*. 1972;56:2142–2160.
- [63] Spiering H. Elastic interaction in spin-crossover compounds. In: Gütlich P, Goodwin HA, editors. *Top curr chem*. Berlin Heidelberg: Berlin Heidelberg: Springer; 2004. p. 171–195.
- [64] Slimani A, Boukheddaden K, Yamashita K. Effect of intermolecular interactions on the nucleation, growth, and propagation of like-spin domains in spin-crossover materials. *Phys Rev B*. 2015;92:014111.
- [65] Marino A, Buron-Le Cointe M, Lorenc M, et al. Out-of-equilibrium dynamics of photoexcited spin-state concentration waves. *Faraday Discuss*. 2015;177:363–379.
- [66] Traiche R, Sy M, Boukheddaden K. Elastic frustration in 1D spin-crossover chains: evidence of multi-step transitions and self-organizations of the spin states. *J Phys Chem C*. 2018;122:4083–4096.
- [67] Boinnard D, Bousseksou A, Dworkin A, et al. Two-step spin conversion of  $[\text{FeII}(\text{5-NO}_2\text{-sal-N}(1,4,7,10))]$ : 292,153, and 103 K x-ray crystal and molecular structure, infrared, magnetic, Moessbauer, calorimetric, and theoretical studies. *Inorg Chem*. 1994;33:271–281.
- [68] Nishino M, Miyashita S. Effect of the short-range interaction on critical phenomena in elastic interaction systems. *Phys Rev B*. 2013;88:014108.
- [69] Cruddas J, Powell BJ. Structure–property relationships and the mechanisms of multi-step transitions in spin crossover materials and frameworks. *Inorg Chem Front*. 2020;7:4424–4437.
- [70] Trzop E, Zhang D, Pineiro-Lopez L, et al. First step towards a devil’s staircase in spin-crossover materials. *Angew Chem Int Ed Engl*. 2016;55:8675–8679.
- [71] Gütlich P, Garcia Y, Goodwin HA. Spin crossover phenomena in Fe(II) complexes. *Chem Soc Rev*. 2000;29:419–427.
- [72] Kusz J, Zubko M, Neder RB, et al., Structural phase transition to disorder low-temperature phase in  $[\text{Fe}(\text{ptz})_6](\text{BF}_4)_2$  spin-crossover compounds. *Acta Crystallogr B*. 2012. 68:40–56.
- [73] Marino A, Chakraborty P, Servol M, et al. The role of ligand- field states in the ultrafast photophysical cycle of the prototypical Iron(II) spin- crossover compound  $[\text{Fe}(\text{ptz})_6](\text{BF}_4)_2$ . *Angew Chem-Int Ed*. 2014;53:3863–3867.
- [74] Chong C, Mishra H, Boukheddaden K, et al. Electronic and structural aspects of spin transitions observed by optical microscopy. The case of  $[\text{Fe}(\text{ptz})_6](\text{BF}_4)_2$ . *J Phys Chem B*. 2010;114:1975–1984.
- [75] Goujon A, Varret F, Boukheddaden K, et al. An optical microscope study of photo-switching and relaxation in single crystals of the spin transition solid  $[\text{Fe}(\text{ptz})_6](\text{BF}_4)_2$ , with image processing. *Inorganica Chim Acta*. 2008;361:4055–4064.

- [76] Hauser A. Cooperative effects on the Hs -] Ls relaxation in the  $[\text{Fe}(\text{ptz})_6](\text{BF}_4)_2$  spin-crossover system. *Chem Phys Lett.* **1992**;192:65–70.
- [77] Hauser A. Intersystem crossing in the  $[\text{Fe}(\text{ptz})_6](\text{BF}_4)_2$  spin crossover system (Ptz = 1-Propyltetrazole). *J Chem Phys.* **1991**;94:2741–2748.
- [78] Lakhloufi S, Guionneau P, Lemée-Cailleau MH, et al. Structural phase transition in the spin-crossover complex  $[\text{Fe}(\text{ptz})_6](\text{BF}_4)_2$  studied by x-ray diffraction. *Phys Rev B.* **2010**;82:132104.
- [79] Carpenter MA, Salje EKH, Graeme-Barber A. Spontaneous strain as a determinant of thermodynamic properties for phase transitions in minerals. *Eur J Mineral.* **1998**;10:621–691.
- [80] Salje EK. Phase transitions in ferroelastic and co-elastic crystals. Cambridge: Cambridge University Press; **1991**.
- [81] Lemée-Cailleau M-H, Ecolivet C, Ouladdiaf B, et al. Multi-phase spin crossover in  $[\text{Fe}(\text{ptz})_6](\text{BF}_4)_2$ . *Phys B Condens Matter.* **2009**;404:379–381.
- [82] Jeftić J, Romstedt H, Hauser A. The interplay between the spin transition and the crystallographic phase transition in the fe(II) spin-crossover system  $[\text{Zn}_{1-x}\text{Fe}_x(\text{ptz})_6](\text{BF}_4)_2$  ( $x = 0.1, 1$ ; ptz= 1-propyltetrazole). *J Phys Chem Solids.* **1996**;57:1743–1750.
- [83] Jeftić J, Hauser A. Pressure study of the thermal spin transition and the high-spin  $\rightarrow$  low-spin relaxation in the R3 and PT crystallographic phases of  $[\text{Zn}_{1-x}\text{Fe}_x(\text{ptz})_6](\text{BF}_4)_2$  single crystals ( $x = 0.1, 0.32, \text{ and } 1$ ; ptz = 1-n-propyltetrazole). *J Phys Chem A.* **1997**;101:10262–10270.
- [84] Azzolina G, Bertoni R, Collet E. General Landau theory of non-symmetry-breaking and symmetry-breaking spin transition materials. *J Appl Phys.* **2021**;129:085106.
- [85] Törnroos KW, Hostettler M, Chernyshov D, et al. Interplay of spin conversion and structural phase transformations: re-entrant phase transitions in the 2-propanol solvate of tris(2-picolyamine)iron(II) dichloride. *Chem Eur J.* **2006**;12:6207–6215.
- [86] Money VA, Elhaik J, Radosavljevic Evans I, et al. A study of the thermal and light induced spin transition in  $[\text{FeL}_2](\text{BF}_4)_2$  and  $[\text{FeL}_2](\text{ClO}_4)_2$  L = 2,6-di(3-methylpyrazol-1-yl)pyrazine. *Dalton Trans.* **2004**;1:65–69.
- [87] Craig GA, Sánchez Costa J, Roubeau O, et al. Coupled crystallographic order–disorder and spin state in a bistable molecule: multiple transition dynamics. *Chem Eur J.* **2011**;17:3120–3127.
- [88] Djemel A, Stefanczyk O, Marchivie M, et al. Solvatomorphism-induced 45 K hysteresis width in a spin-crossover mononuclear compound. *Chem Eur J.* **2018**;24:14760–14767.
- [89] Azzolina G, Bertoni R, Ecolivet C, et al. Landau theory for non-symmetry-breaking electronic instability coupled to symmetry-breaking order parameter applied to Prussian blue analog. *Phys Rev B.* **2020**;102:134104.
- [90] Floquet S, Guillou N, Négrier P, et al. The crystallographic phase transition for a ferric thiosemicarbazone spin crossover complex studied by X-ray powder diffraction. *New J Chem.* **2006**;30:1621–1627.
- [91] Weber B, Kaps ES, Obel J, et al. Synthesis and characterization of a dinuclear iron(II) spin crossover complex with wide hysteresis. *Inorg Chem.* **2008**;47:10779–10787.
- [92] Zhu -Y-Y, Liu C-W, Yin J, et al. Structural phase transition in a multi-induced mononuclear FeII spin-crossover complex. *Dalton Trans.* **2015**;44:20906–20912.
- [93] Seredyuk M, Muñoz MC, Castro M, et al. Unprecedented multi-stable spin crossover molecular material with two thermal memory channels. *Chem Eur J.* **2013**;19:6591–6596.
- [94] Halcrow MA. Spin-crossover compounds with wide thermal hysteresis. *Chem Lett.* **2014**;43:1178–1188.

- [95] Reeves MG, Tailleux E, Wood PA, et al. Mapping the cooperativity pathways in spin crossover complexes. *Chem Sci.* **2021**;12:1007–1015.
- [96] Collet E, Guionneau P. Structural analysis of spin-crossover materials: from molecules to materials. *Cr Chim.* **2018**;21:1133–1151.
- [97] Serebyuk M, Znovjyak K, Valverde-Muñoz FJ, et al. Spin transition and symmetry-breaking in new mononuclear FeII tren-complexes with up to 38 K hysteresis around room temperature. *Inorg Chem Front.* **2022**;9:537–546.
- [98] Paliwoda D, Vendier L, Nicolazzi W, et al. Pressure tuning of coupled structural and spin state transitions in the molecular complex [Fe(H<sub>2</sub>B(pz)<sub>2</sub>)<sub>2</sub>(phen)]. *Inorg Chem.* **2022**;61:15991–16002.
- [99] Collet E, Azzolina G. Coupling and decoupling of spin crossover and ferroelastic distortion: unsymmetric hysteresis loop, phase diagram, and sequence of phases. *Phys Rev Mater.* **2021**;5:044401.
- [100] Watanabe H, Hirori H, Molnár G, et al. Temporal decoupling of spin and crystallographic phase transitions in Fe(ptz)<sub>6</sub>(BF<sub>4</sub>)<sub>2</sub>. *Phys Rev B.* **2009** 79; 180405(R).
- [101] Ohkoshi S, Tokoro H, Matsuda T, et al. Coexistence of ferroelectricity and ferromagnetism in a rubidium manganese hexacyanoferrate. *Angew Chem.* **2007**;46:3238–3241.
- [102] Collet E, Lemee-Cailleau MH, Buron-Le Cointe M, et al. Laser-induced ferroelectric structural order in an organic charge-transfer crystal. *Science.* **2003**;300:612–615.
- [103] Perlepe P, Oyarzabal I, Mailman A, et al. Metal-organic magnets with large coercivity and ordering temperatures up to 242°C. *Science.* **2020**;370:587–592.
- [104] Shatruk M, Phan H, Chrisostomo BA, et al. Symmetry-breaking structural phase transitions in spin crossover complexes. *Coord Chem Rev.* **2015**;289–290:62–73.
- [105] Ortega-Villar N, Muñoz CM, Real AJ. Symmetry breaking in iron(II) spin-crossover molecular crystals. *Magnetochemistry.* **2016**;2:1.
- [106] Ohkoshi S, Imoto K, Tsunobuchi Y, et al. Light-induced spin-crossover magnet. *Nat Chem.* **2011**;3:564–569.
- [107] Wiehl L. Structures of hexakis(1-propyltetrazole)iron(II) bis(tetrafluoroborate), [Fe(CHN<sub>4</sub>C<sub>3</sub>H<sub>7</sub>)<sub>6</sub>](BF<sub>4</sub>)<sub>2</sub>, hexakis(1-methyltetrazole)iron(II) bis(tetrafluoroborate), [Fe(CHN<sub>4</sub>CH<sub>3</sub>)<sub>6</sub>](BF<sub>4</sub>)<sub>2</sub>, and the analogous perchlorates. Their relation to spin crossover behaviour and comparison of Debye-Waller factors from structure determination and Mossbauer spectroscopy. *Acta Crystallogr B.* **1993**;49:289–303.
- [108] Wiehl L, Spiering H, Gutlich P, et al. Calculation of the lattice deformation at the phase transitions of [Fe(ptz)<sub>6</sub>](BF<sub>4</sub>)<sub>2</sub> from powder diffraction patterns. *J Appl Crystallogr.* **1990**;23:151–160.
- [109] Ozarowski A, McGarvey BR. EPR study of manganese(II) and copper(II) in single crystals of the spin-crossover complex hexakis(1-propyltetrazole)iron(2+) tetrafluoroborate(1-). *Inorg Chem.* **1989**;28:2262–2266.
- [110] Jung J, Bruchhäuser F, Feile R, et al., The cooperative spin transition in [FexZn1 – x(ptz)<sub>6</sub>](BF<sub>4</sub>)<sub>2</sub>: i. Elastic properties — an oriented sample rotation study by Brillouin spectroscopy. *Zeitschrift für Physik B Condens Mat.* **1996.** 100:517–522.
- [111] Jung J, Schmitt G, Wiehl L, et al., The cooperative spin transition in [FexZn1 – x(ptz)<sub>6</sub>](BF<sub>4</sub>)<sub>2</sub>: II. Structural properties and calculation of the elastic interaction. *Zeitschrift für Physik B Condens Mat.* **1996.** 100:523–534.
- [112] Chakraborty P, Sy M, Fourati H, et al. Optical microscopy imaging of the thermally-induced spin transition and isothermal multi-stepped relaxation in a low-spin stabilized spin-crossover material. *Phys Chem Chem Phys.* **2022**;24:982–994.

- [113] Axe JD, Yamada Y. Cubic-tetragonal elastic phase transformations in solids. *Phys Rev B*. **1981**;24:2567–2569.
- [114] Janovec V, Privratska J. Domain structures. *Int Tables Crystallogr*. **2006**;D:449–505.
- [115] Janovec V, Dvořák V, Petzelt J. Symmetry classification and properties of equi-translation structural phase transitions. *Czechoslov J Phys*. **1975**. 25:1362–1396.
- [116] Toledano P, Fejer MM, Auld BA. Nonlinear elasticity in proper ferroelastics. *Phys Rev B*. **1983**;27:5717–5746.
- [117] Chernyshov D, Bürgi H-B, Hostettler M, et al. Landau theory for spin transition and ordering phenomena in Fe(II) compounds. *Phys Rev B*. **2004**;70:094116.